On the Analysis of Ductile Fracture Mechanisms

VIGGO TVERGAARD
Department of Solid Mechanics, The Technical University of Denmark, Lyngby, Denmark

ABSTRACT

Various approaches to the study of ductile fracture in metals are discussed, including the application of dilatant plasticity theories and a number of analyses for representative unit volumes containing a single void. The porous ductile material model discussed is a kinematic/isotropic hardening version that can be used to represent the formation of a rounded vertex on subsequent yield surfaces, and this model is used to study the interaction of two size-scales of voids. Model studies for the effect of nucleation are presented, and a viscoplastic version of the porous ductile material model is used to represent the brittle ductile transition.

KEYWORDS

Ductile fracture; voids; softening; rate sensitivity.

INTRODUCTION

Failure in ductile metals occurs mainly by coalescence of microscopic voids. The voids tend to nucleate at second phase particles, by decohesion of the particle-matrix interface or by particle fracture, and subsequently they grow due to large plastic deformation of the surrounding metal matrix. When adjacent voids are sufficiently large relative to their spacing, they interact strongly and finally coalesce as the ligament necks down. In some cases localization of plastic flow in a shear band occurs prior to coalescence so that subsequent nucleation and void growth takes place only inside the band, leading to a so-called void-sheet failure.

Constitutive relations that account for porosity in ductile materials have been proposed by various authors. The most well-known model is that developed by Gurson (1977), based on micro-mechanical studies, which has been improved subsequently by various authors. To also account for the effect of a rounded vertex that often develops on subsequent yield surfaces at the point of loading, Mear and Hutchinson (1985) have suggested a kinematic hardening version of the porous material model. This model, extended to

account for void nucleation (Tvergaard, 1987a), is presented in the present paper.

Analyses of the behaviour of a characteristic unit-volume containing a single void are an important tool in the understanding of porous ductile material behaviour. Results of a number of such analyses are discussed here, representing periodic arrays of circular cylindrical voids or spherical voids. For a void in a pure shear field the void volume decays, and here the particle remaining inside the void after nucleation plays an important role. Furthermore, the interaction of two size scales of voids is illustrated by results of a full 3D numerical analysis for a periodic array of spherical larger voids, with both size scales of voids represented in terms of the porous ductile material model.

The brittle ductile transition in structural alloys results from the competition between two fracture mechanisms, cleavage and void coalescence, while the difference between transition temperatures at impact loading and slow loading, respectively, is a result of material strain-rate sensitivity. A material model that includes these additional effects is briefly discussed and illustrated by numerical results (Tvergaard and Needleman, 1986,1988) obtained for Charpy V-notch specimens.

CONTINUUM MODEL FOR POROUS DUCTILE SOLIDS

For a ductile material containing a certain volume fraction of micro-voids Gurson (1977) has developed a material model, based on averaging techniques analogous to those applied to a polycrystalline aggregate by Bishop and Hill (1951). The unit cube considered by Gurson (1977) is an aggregate of voids and rigid plastic material, and approximate upper-bound solutions on the micro-level have been used to derive a macroscopic yield condition.

In the present paper the ductile porous material model will be presented in terms of a generalized form suggested by Mear and Hutchinson (1985), who introduced a family of isotropic/kinematic hardening yield surfaces of the form $\Phi(\sigma^{ij} , \alpha^{ij} , \sigma_F , f) = 0$, where f is the current void volume fraction, σ^{ij} is the average macroscopic Cauchy stress tensor and α^{ij} denotes the center of the yield surface. The radius σ_F of the yield surface for the matrix material is taken to be given by

$$\sigma_F = (1 - b)\sigma_y + b\,\sigma_M \tag{1}$$

where σ_y and σ_M are the initial yield stress and the matrix flow stress, respectively, and the parameter b is a constant in the range $[0 , 1]$. This material model was extended by Tvergaard (1987a) to account for void nucleation. The constitutive relations are formulated such that for $b = 1$ they reduce to Gurson's (1977) isotropic hardening model, whereas a pure kinematic hardening model appears for $b = 0$.

The approximate yield condition used is of the form

$$\Phi = \frac{\tilde{\sigma}_e^2}{\sigma_F^2} + 2q_1 f^* \cosh\left\{\frac{\tilde{\sigma}_k^k}{2\sigma_F}\right\} - 1 - (q_1 f^*)^2 = 0 \tag{2}$$

where

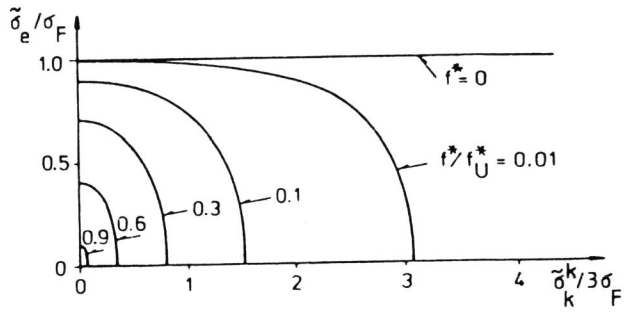

Fig. 1. Yield surface dependence on the value of $f^*(f)$ in (2).

$$\tilde{\sigma}^{ij} = \sigma^{ij} - \alpha^{ij} , \quad \tilde{\sigma}_e = (3\tilde{s}^{ij}\tilde{s}_{ij}/2)^{1/2} , \quad \tilde{s}^{ij} = \tilde{\sigma}^{ij} - G^{ij}\tilde{\sigma}_k^k/3 \tag{3}$$

For $f^* = f$ and $q_1 = 1$ the expression (2) is that proposed by Mear and Hutchinson (1985), which coincides with that of Gurson (1977) if $b = 1$. The parameter q_1 (> 1) was proposed by Tvergaard (1981,1982a) to bring predictions of the model at low void volume fractions in closer agreement with full numerical analyses for periodic arrays of voids. The function $f^*(f)$ in (2) was introduced by Tvergaard and Needleman (1984) to model the more rapid loss of material stress carrying capacity associated with void coalescence (see Fig. 1). This function was chosen as

$$f^*(f) = \begin{cases} f & , \text{ for } f \le f_C \\ f_C - \dfrac{f_U^* - f_C}{f_F - f_C}(f - f_C) & , \text{ for } f > f_C \end{cases} \tag{4}$$

so that the modification becomes active when f exceeds a certain critical value f_C , and final fracture occurs for $f = f_F$ (i.e. $f^*(f_F) = f_U^* = 1/q_1$) . Based on experimental results and numerical model analyses the values $f_C = 0.15$ and $f_F = 0.25$ were chosen (Tvergaard and Needleman, 1984), and many investigations have used the value $q_1 = 1.5$.

Equations are given here in the context of a Lagrangian formulation of the field equations, in which a material point is identified by the coordinates x^i in the reference configuration. The metric tensors in the current configuration and the reference configuration are denoted G_{ij} and g_{ij} , respectively, with determinants G and g , and η_{ij} denotes the Lagrangian strain tensor. The contravariant components of the Cauchy stress

tensor σ^{ij} and the Kirchhoff stress tensor τ^{ij} on the embedded deformed coordinates are related by the expression $\tau^{ij} = \sqrt{G/g}\,\sigma^{ij}$. Indices range from 1 to 3 , and the summation convention is adopted for repeated indices.

The plastic part of the macroscopic strain increment $\dot{\eta}^{P}_{ij}$ and the effective plastic strain increment $\dot{\epsilon}^{P}_{M}$ for the matrix material are taken to be related by (see Tvergaard, 1987a)

$$\tilde{\sigma}^{ij}\,\dot{\eta}^{P}_{ij} = (1 - f)\sigma_F\,\dot{\epsilon}^{P}_{M} \tag{5}$$

For $f = 0$ (5) is an exact relationship for the classical kinematic hardening solid, and for $b = 1$ the expression reduces to the equivalent plastic work expression applied by Gurson (1977). Substituting the uniaxial true stress natural strain curve for the matrix material, $\dot{\epsilon}^{P}_{M} = (1/E_t - 1/E)\dot{\sigma}_M$, into (5) gives

$$\dot{\sigma}_M = \frac{EE_t}{E - E_t}\,\frac{\tilde{\sigma}^{ij}\,\dot{\eta}^{P}_{ij}}{(1 - f)\sigma_F} \tag{6}$$

where E and E_t are Young's modulus and the tangent modulus, respectively.

In the studies to be discussed here the uniaxial true stress-logarithmic strain curve for the matrix material will be represented by the piecewise power law

$$\epsilon = \begin{cases} \dfrac{\sigma}{E} & , \quad \text{for } \sigma < \sigma_y \\[2ex] \dfrac{\sigma_y}{E}\left(\dfrac{\sigma}{\sigma_y}\right)^n & , \quad \text{for } \sigma \geq \sigma_y \end{cases} \tag{7}$$

where n is the strain hardening exponent.

The change of the void volume fraction during an increment of deformation is taken to be given by

$$\dot{f} = (\dot{f})_{growth} + (\dot{f})_{nucleation} \tag{8}$$

The increment due to growth is

$$(\dot{f})_{growth} = (1 - f)G^{ij}\,\dot{\eta}^{P}_{ij} \tag{9}$$

since the matrix material is plastically incompressible. Nucleation of new voids occurs mainly at second phase particles, by decohesion of the particle-matrix interface or by particle fracture, and Needleman and Rice (1978) have suggested a nucleation model of the form

$$(\dot{f})_{nucleation} = A\,\dot{\sigma}_M + B\,(\sigma^k_k)^{\cdot}/3 \tag{10}$$

A fictitious Gurson yield surface $\Phi_G = \Phi_G(\sigma^{ij}_G\ ,\ \sigma_M\ ,\ f)$ was used by Tvergaard (1987a) to formulate the constitutive relations, where σ_M and f are the current values, and σ^{ij}_G are a set of fictitious stress components chosen such that

$$\frac{\sigma^{ij}_G}{\sigma_M} = \frac{\tilde{\sigma}^{ij}}{\sigma_F} \tag{11}$$

With this assumption, $\Phi_G = 0$ is a direct consequence of $\Phi = 0$. In most cases the fictitious stresses σ^{ij}_G will differ from the actual stresses σ^{ij} at every point of the current yield surface.

The expression for $\dot{\eta}^{P}_{ij}$ in a point of the yield surface $\Phi = 0$ is chosen identical to that given by the Gurson model at the point σ^{ij}_G of the fictitious surface $\Phi_G = 0$. Thus, the plastic part of the macroscopic strain increment is taken to be

$$\dot{\eta}^{P}_{ij} = \frac{1}{H}\,m^{G}_{ij}\,m^{F}_{k\ell}\,\overset{\nabla}{\sigma}{}^{k\ell} \tag{12}$$

where

$$m^{G}_{ij} = \frac{3}{2}\frac{\tilde{s}_{ij}}{\sigma_F} + \alpha\,G_{ij}\quad ,\quad m^{F}_{ij} = \frac{3}{2}\frac{\tilde{s}_{ij}}{\sigma_F} + \beta\,G_{ij} \tag{13}$$

$$\alpha = \frac{f^*}{2}\,q_1\,\sinh\left[\frac{\tilde{\sigma}^k_k}{2\sigma_F}\right]\quad ,\quad \beta = \alpha + \frac{B\sigma_M}{6}\,\frac{\partial\Phi}{\partial f} \tag{14}$$

$$H = \frac{\sigma_M}{2}\left[-3\alpha(1-f)\frac{\partial\Phi}{\partial f} - \left\{\frac{\partial\Phi}{\partial f}A + \frac{\sigma_F}{\sigma_M}\,\frac{\partial\Phi}{\partial\sigma_F}\right\}\frac{EE_t}{E-E_t}\,\frac{1}{1-f}\left[\frac{\tilde{\sigma}^2_e}{\sigma^2_F} + \alpha\,\frac{\tilde{\sigma}^k_k}{\sigma_F}\right]\right] \tag{15}$$

Plastic yielding initiates when $\Phi = 0$ and $\dot{\Phi} > 0$ during elastic deformation, and continued plastic loading requires $\Phi = 0$ and $\frac{1}{H}\,m^{F}_{k\ell}\,\overset{\nabla}{\sigma}{}^{k\ell} \geq 0$.

The evolution equation for the yield surface centre during a plastic increment is taken to be

$$\overset{\nabla}{\alpha}{}^{ij} = \dot{\mu}\,\tilde{\sigma}^{ij}\quad ,\quad \dot{\mu} \geq 0 \tag{16}$$

which is a finite strain generalization of Ziegler's (1959) hardening rule. The value of the parameter $\dot{\mu}$ is determined so that the consistency condition, $\dot{\Phi} = 0$, is satisfied

$$\dot{\mu} = (1-b)\frac{1}{2}\left[\frac{\tilde{\sigma}_e^2}{\sigma_F^2} + \alpha\,\frac{\tilde{\sigma}_k^k}{\sigma_F}\right]^{-1}\left[\frac{2}{\sigma_F}\,m^G_{k\ell}\,\overset{\nabla}{\sigma}{}^{k\ell} + \frac{\sigma_y}{\sigma_F}\,\frac{\partial\Phi}{\partial f}\,\frac{\mathscr{B}}{3}\,G_{k\ell}\,\overset{\nabla}{\sigma}{}^{k\ell}\right.$$

$$\left. + \frac{\sigma_y}{\sigma_F}\,\frac{1}{H}\,\frac{\partial\Phi}{\partial f}\left\{3\alpha(1-f) + \mathscr{A}\,\frac{EE_t}{E-E_t}\,\frac{1}{1-f}\left[\frac{\tilde{\sigma}_e^2}{\sigma_F^2} + \alpha\,\frac{\tilde{\sigma}_k^k}{\sigma_F}\right]\right\} m^F_{k\ell}\,\overset{\nabla}{\sigma}{}^{k\ell}\right] \tag{17}$$

In cases where large rotations of the principal stress axes occur relative to the material, the finite strain generalization (16) in terms of the Jaumann rate may give a poor representation of material behaviour, and other corotational rates may be preferable (Dafalias, 1983; Lee *et al.*, 1983). However, in shear localization studies the rotations of the principal stress axes prior to localization are quite small, and for such studies Mear and Hutchinson (1985) have found that using the Dienes rate makes little difference.

Materials, in which nucleation is controlled by the maximum normal stress on the particle-matrix interface, are modelled (Needleman and Rice, 1978) by using the sum $\sigma_M + \sigma_k^k/3$ as an approximate measure of this maximum stress, thus taking $\mathscr{A} = \mathscr{B}$ in (10). Chu and Needleman (1980) have suggested a normal distribution for nucleation, so that $\mathscr{A}$ and $\mathscr{B}$ are given by

$$\left.\begin{aligned} \mathscr{A} = \mathscr{B} &= \frac{f_N}{s\sqrt{2\pi}}\,e^{-\frac{1}{2}\left\{\frac{(\sigma_M + \sigma_k^k/3) - \sigma_N}{s}\right\}^2} \\ \text{for}\quad \sigma_M + \sigma_k^k/3 &= (\sigma_M + \sigma_k^k/3)_{max} \quad\text{and}\quad (\sigma_M + \sigma_k^k/3)^{\cdot} > 0 \end{aligned}\right\} \tag{18}$$

where σ_N is the mean stress for nucleation, s is the corresponding standard deviation, and f_N is the volume fraction of void nucleating particles.

A material, in which nucleation is controlled by the plastic strain ϵ^P_M, can be modelled in terms of (10) by taking $\mathscr{A} > 0$ and $\mathscr{B} = 0$. Again assuming a normal distribution, the expression for $\mathscr{A}$ is analogous to (18), with ϵ_N and s denoting the mean strain for nucleation and the corresponding standard deviation, respectively.

The incremental constitutive relations are obtained by assuming that the total strain rate is the sum of the elastic and plastic parts, $\dot{\eta}_{ij} = \dot{\eta}^E_{ij} + \dot{\eta}^P_{ij}$, and using the elastic relationship $\overset{\nabla}{\sigma}{}^{ij} = \mathscr{R}^{ijk\ell}\,\dot{\eta}^E_{k\ell}$. This leads to incremental constitutive relations of the form (Tvergaard, 1982c)

$$\overset{\cdot}{\tau}{}^{ij} = \left[\mathscr{L}^{ijk\ell} - \gamma\,M^{ij}_G M^{k\ell}_F\right]\dot{\eta}_{k\ell} \tag{19}$$

where

$$\mathscr{L}^{ijk\ell} = \sqrt{\frac{G}{g}}\left[\mathscr{R}^{ijk\ell} - \frac{1}{2}(\sigma^{ik}G^{j\ell} + \sigma^{jk}G^{i\ell} + \sigma^{i\ell}G^{jk} + \sigma^{j\ell}G^{ik}) + \sigma^{ij}G^{k\ell}\right] \tag{20}$$

$$M^{ij}_G = \mathscr{R}^{ijk\ell}\,m^G_{k\ell}\quad,\quad M^{k\ell}_F = m^F_{rs}\,\mathscr{R}^{rsk\ell} \tag{21}$$

$$\gamma = \begin{cases} 0 & \text{, for elastic unloading} \\ \sqrt{\frac{G}{g}}\left[H + m^F_{rs}\,\mathscr{R}^{rsk\ell}\,m^G_{k\ell}\right]^{-1} & \text{, for plastic loading} \end{cases} \tag{22}$$

MODEL STUDIES FOR PERIODIC ARRAYS OF VOIDS

Detailed micro-mechanical analyses for characteristic unit volumes with known void volume fraction have been an important tool in the understanding of the influence of porosity in ductile materials.

Effect of porosity

An early numerical analysis of this type was carried out by Needleman (1972) for a square array of circular cylindrical voids. Here, the consideration of a periodic array of voids is important, since this allows for the assumption of a periodic solution, where only a small subregion has to be analysed. The same type of method has been used in a recent analysis by Guennouni and Francois (1987).

An axisymmetric model problem, with a circular cylindrical body containing a single spherical void, has been used by Tvergaard (1982a) to represent a periodic array of spherical voids. Such adjacent cylindrical bodies are not compatible, but the application of axisymmetry facilitates the analysis significantly, and it has been assumed that the solutions for hexagonal cylinders (see Fig. 2) are reasonably well approximated by the axisymmetric solutions. Also a spherical body with a concentric spherical void has been used in a number of model studies, again assuming that the solutions are reasonably good approximations in spite of incompatibilities between adjacent spherical bodies.

The upper-bound rigid plastic model analyses used by Gurson (1977) to derive the approximate yield condition of the form (2), for $b = 1$ and $q_1 = 1$, were based on a spherical body with a concentric spherical void.

Subsequently, numerical studies for the square array of circular cylindrical voids, as well as the periodic array of spherical voids represented by cylindrical model problems, have been used to investigate this porous material model, and localization studies for these two types of model problems have been the basis of introducing the additional parameter $q_1 \simeq 1.5$ in (2). Critical strains, nominal tractions and band inclinations at shear band bifurcation found by Tvergaard (1981) are shown in Fig. 3 for uniaxial plane strain tension, comparing results of cell model studies (square array of cylindrical voids) with predictions of the continuum model for $q_1 = 1.5$ (solid curves). The chosen value of q_1 larger than unity gives a signifi-

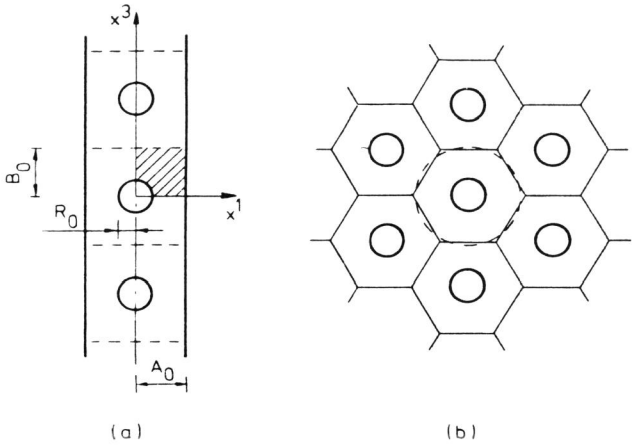

Fig. 2. Axisymmetric model of a material containing spherical voids.

cant improvement, but no perfect fit, and this level of agreement is supported by the comparisons of Tvergaard (1982a) and in a number of more recent papers.

Since the model studies tend to focus on periodic arrays of voids, an experimental investigation by Magnusen *et al.* (1987) for the effect of the void distribution is of significant interest. A series of tensile tests have been carried out for specimens with either random or regular arrays of cylindrical holes drilled through the thickness, where the volume fraction

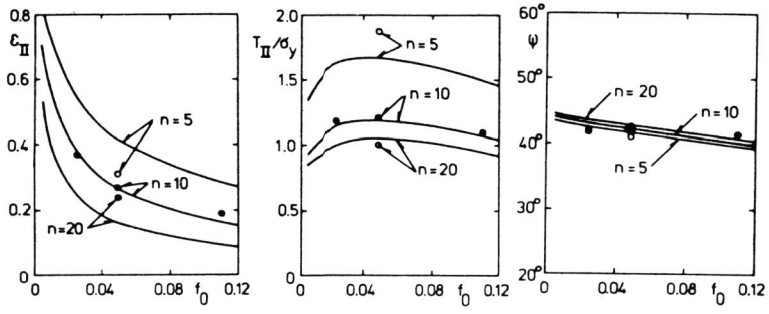

Fig. 3. Shear band bifurcation predictions for periodic array of voids under uniaxial plane strain tension, compared with continuum model (solid curves) for $b = 1$ and $q_1 = 1.5$. Logarithmic strain, nominal traction and angle of band inclination vs. initial void volume fraction (Tvergaard, 1981).

of holes is the same in all cases. The degree of randomness was controlled by specifying a minimum hole spacing, and it was found that the fracture strain is smaller the more randomness is allowed, while a regular square array of holes gave the maximum fracture strain. On the other hand, the effect of randomness on the behaviour prior to final failure was much smaller.

Softening due to nucleation

One consequence of void nucleation is a reduction of the macroscopic strain hardening capacity during the process of nucleation. Since plastic instabilities depend strongly on the values of the instantaneous moduli this reduced hardening can result in instabilities that are precursors of final failure. In fact, based on the Gurson model Needleman and Rice (1978) have demonstrated that a burst of nucleation can result in very early localization of plastic flow in a shear band. Such localization may lead to shear fracture, but analyses carried beyond the initial onset of localization (Tvergaard, 1982c) have shown that in some cases the localized plastic flow stops once the burst of nucleation is over.

Model studies to get a more detailed understanding of the softening behaviour associated with nucleation have been carried out by Hutchinson and Tvergaard (1987). Some of these studies were carried out for an isolated spherical void in an infinite matrix, to represent situations where the interaction between adjacent voids is negligible. Other studies were carried out using the axisymmetric model problem illustrated in Fig. 2. In all cases nucleation at some given level of macroscopic stress or strain was modelled by incrementally reducing the traction across the particle/matrix interface to zero. No attempt was made to model the actual process of interfacial decohesion, since the main focus was the effect of nucleation on macroscopic material behaviour.

Nucleation of an isolated void at macroscopic stresses Σ_{ij} that have been applied proportionally, result in stress redistribution and additional straining of the matrix. The additional macroscopic straining during the nucleation of the void volume fraction $\dot{f}$ is denoted by $\dot{f}\Delta E_{ij}$, such that $\Sigma_{ij}\dot{f}\Delta E_{ij}$ is the extra work done by the remote stress due to nucleation. Thus, in the presence of nucleation the strain increments are given by

$$\dot{E}_{ij} = M_{ijk\ell}\,\dot{\Sigma}_{k\ell} + \dot{f}\Delta E_{ij} \tag{23}$$

where $M_{ijk\ell}$ are the incremental compliances corresponding to $\dot{f} = 0$. Numerical results for a spherical void in an isotropic hardening Mises material are well approximated by an expression of the form (Hutchinson and Tvergaard, 1987)

$$\Delta E_{ij} = \frac{1}{E_t}\,F\left[\frac{\Sigma_m}{\Sigma_e}\right]\Sigma'_{ij} + \frac{1}{E}\,G\left[\frac{\Sigma_m}{\Sigma_e}\right]\Sigma_m\,\delta_{ij} \tag{24}$$

where Σ_m and Σ_e are the macroscopic mean stress and Mises stress, respectively, and Σ'_{ij} is the stress deviator.

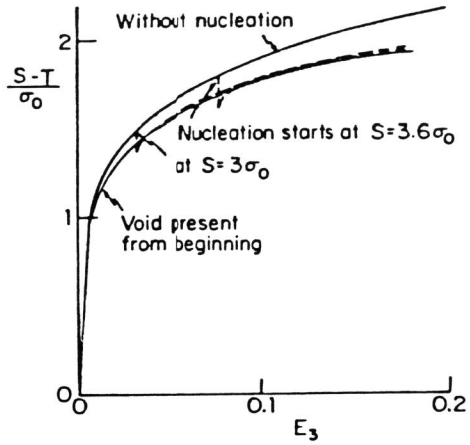

Fig. 4. Effect of nucleation at constant axial strain for fixed ratio $T/S = 0.5$ of radial and axial macroscopic stresses (Hutchinson *et al.*, 1987).

The functions F and G depend mainly on Σ_m/Σ_e, but there is also a weak dependence on the total strain increment during nucleation and on the ratio E_t/E. Since $1/E_t$ is generally much larger than $1/E$ and F is much larger than G, it is clear from (24) that the deviatoric contribution to ΔE_{ij} is much larger than that of dilatation. A comparison with the Gurson model, (1)-(15) for $b = 1$, shows that the numerically determined values of F are reasonably well represented by the Gurson model, while this model neglects the dilatant contribution to ΔE_{ij} (i.e. $G = 0$).

The effect of a uniform distribution of spherical particles that nucleate voids simultaneously has been studied by analysing the axisymmetric model problem illustrated in Fig. 2. The volume fraction of rigid spherical particles is chosen as 0.01 and the analyses are carried out for a relatively high stress triaxiality, with a fixed ratio 0.5 between radial and axial macroscopic true stresses. In this stress state the void expands everywhere as soon as the interfacial forces are relaxed, so that matrix-particle interaction after nucleation is not an issue. If nucleation occurs at constant macroscopic stress, $\dot{\Sigma}_{ij} = 0$, the additional strains in (23) are directly obtained, and the corresponding values of F and G computed from (24) have been found to agree reasonably with those determined for an isolated void. When nucleation takes place at constant macroscopic strain, the stresses decay to values somewhat below the curve for a void present from the beginning (Fig. 4), while elastic unloading takes place in a great deal of the matrix material near the voids. After a small amount of further stretching these unloading regions disappear, and the stress-strain curve is slightly above that for voids present from the start.

These nucleation model studies have shown that the macroscopic hardening rate is strongly reduced during nucleation, and that a burst of nucleation

can even give negative hardening.

Void growth in shear

The growth of an isolated void in a block of material undergoing simple shearing with superimposed hydrostatic tension has been analysed by Fleck and Hutchinson (1986) for viscous solids, considering both linear viscosity and nonlinear viscosity (power law creep). An important result of these analyses is that in a shear field an initially spherical or circular cylindrical void tends to close as the shear strain grows large. Possibly, void closure would be expected at large shear strains, when the mean stress is zero, but this also occurs at a positive mean stress as large as about half the applied shear stress. This behaviour is not accounted for in the porous material model discussed in the first section of this paper, nor in (24), where void growth is associated with a positive mean stress.

The fact that the voids try to flatten out in a shear field makes the issue of particle matrix interaction central in such studies, subsequent to nucleation. This question has been treated in some detail by Fleck, Hutchinson and Tvergaard (1988). The presence of a particle inside a void has the significant effect that the void volume cannot decrease, and if there is any opening around the particle, the volume must have increased.

Fig. 5 shows the initial mesh and two deformed meshes for a numerical analysis of a material containing a row of constantly spaced circular cylindrical voids, along which final shear fracture is expected to occur. Periodicity conditions are prescribed at the sides of the region analysed (Fig. 5a), symmetry conditions are prescribed at the bottom, and shear stresses Σ_{12} are applied at the top of the region. The solid is elastic-perfectly plastic with yield stress σ_0.

Fig. 6a shows shear stress-strain curves for a case where the particle remains bonded to the matrix material, a case where the void is nucleated at zero strain and the particle remains in sliding contact with part of the void surface, and a case with no particle. The cross-sectional area change of a void, normalized by the initial area, is shown in Fig. 6b. In the case of no particle the void contracts, as already mentioned above, and during this contraction the shear stress slowly increases. The presence of a par-

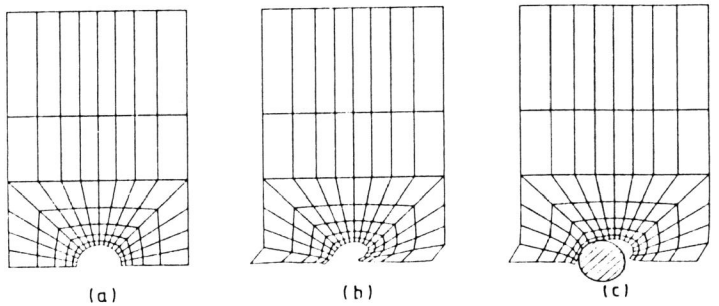

Fig. 5. Initial mesh and two deformed meshes in study of shear failure along row of constantly spaced circular cylindrical voids (Fleck *et al.*, 1988).

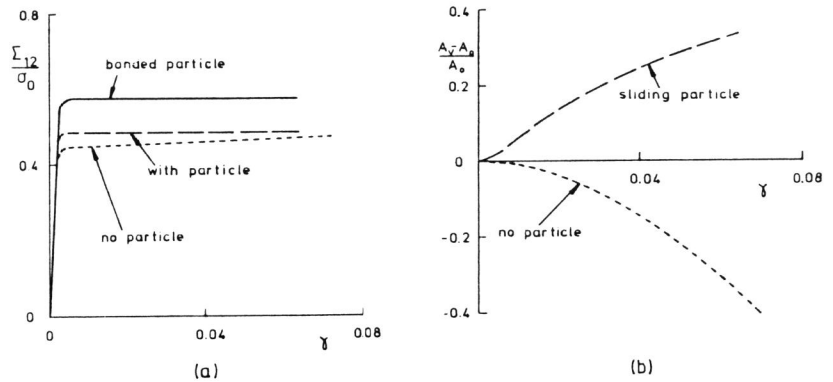

Fig. 6. Shear stress and void growth vs. shear strain for a row of voids in elastic-perfectly plastic material (Fleck *et al.*, 1988).

ticle has a strong influence by enforcing a significant void growth, as can also be seen by comparing the voids in Figs. 5b and c. It has been found by Fleck *et al.* (1988) that a superposed compression on the top of the region analysed (Fig. 5a) increases the difference between the void growth predictions, whereas a superposed tension reduces the difference, until there is no difference when the particle looses contact with the void surface.

Both the void contraction in a material subject to pure shearing and the influence of particle-matrix contact after nucleation are important effects that are usually disregarded in porous material models. This could play an important role in cases where localization of plastic flow in a shear band results in shear fracture by a void sheet mechanism. Further investigations would be necessary to disclose how important these effects are during the coalescence process inside a shear band, dependent on the stress state in the band.

INTERACTION OF TWO SIZE SCALES OF VOIDS

A number of structural alloys contain two size-scales of second phase particles, i.e. a population of relatively large particles with low strength and a population of much stronger small particles. In such materials large voids nucleate at a relatively early stage, while smaller voids nucleate much later, and ductile fracture by void coalescence involves the interaction of the two void populations, as has been observed by Hancock and Mackenzie (1976) for structural steels and by Hahn and Rosenfield (1975) for aluminium alloys. Localization of plastic flow in the matrix material between the larger voids and subsequent void-sheet fracture represents an important mode of final failure in this type of materials.

Plane strain or generalized plane strain analyses of this type of failure mechanism have been carried out (Tvergaard, 1982b) by representing the larger voids as a periodic array of preexisting cylindrical holes and using the Gurson model to represent the small scale voids in the matrix material between the larger voids. A limitation of this plane model is that only

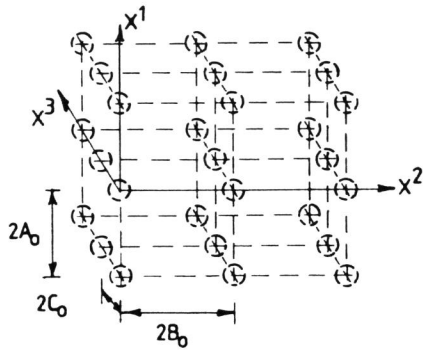

Fig. 7. Model material containing a 3D periodic array of larger spherical inclusions.

cylindrical voids can be represented. An analogous analysis using a cylindrical model problem with a spherical void (Fig. 2) would have the limitation of not being able to represent shear localization between the larger voids.

Recently, a 3-dimensional array of spherical large-scale inclusions has been considered (see Fig. 7), which requires a full 3D numerical analysis of the deformation and damage fields (Tvergaard, 1987b). In addition to the interaction of two different void populations this study also involves the development of a 3D shear band. Previous plane strain localization studies (Tvergaard, Needleman and Lo, 1981) have shown that the accurate representation of a shear band is very dependent on the type of finite elements used, and on the mesh design. Therefore, a box shaped super element is chosen, built up of 24 tetrahedral elements, in such a way that flow localization along 9 different types of planes is allowed for in a regular mesh. Due to periodicity, only the region enclosed by the intervals $[0\ ,\ A_0]$, $[0\ ,\ B_0]$ and $[0\ ,\ C_0]$ on the coordinate axes needs to be analysed numerically.

The porous ductile material model with isotropic/kinematic hardening described in the first section of this paper is used for the analysis. The small strong particles in the matrix material between the larger inclusions are represented by a constant volume fraction f_N^o of void nucleating particles, while each of the large inclusions is represented as an "island" of additional volume fraction Δf_N. Thus, in the vicinity of a large inclusion, with center at the coordinates $(x_0^1\ ,\ x_0^2\ ,\ x_0^3)$ and with radius r_0 the concentration of void nucleating particles is assumed to vary according to

$$f_N = f_N^o + \Delta f_N \exp\left\{-\left[(x^1-x_0^1)^2 + (x^2-x_0^2)^2 + (x^3-x_0^3)^2\right]^2 / r_0^4\right\} \qquad (25)$$

At the larger inclusions, represented by Δf_N, nucleation is assumed to

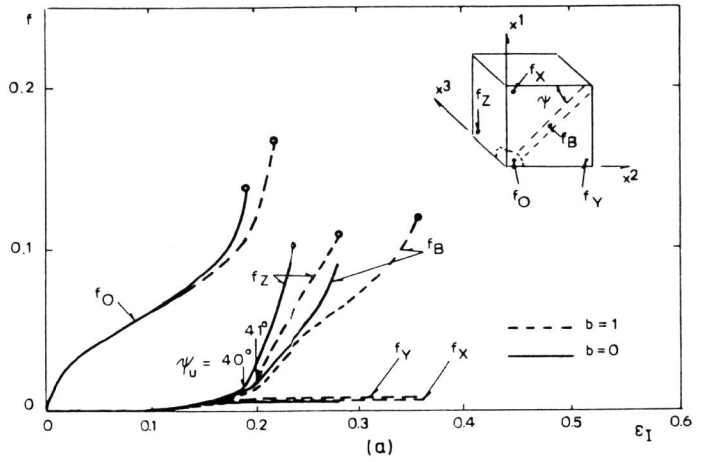

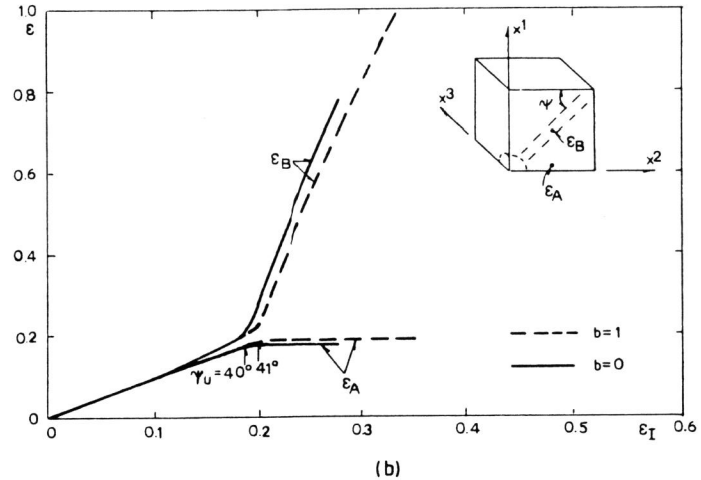

Fig. 8. Development of void volume fractions andprincipal strains vs. average tensile strain, for $\epsilon_{III} = 0$ and $\Sigma_{II} = 0$ (Tvergaard, 1987b).

follow a stress controlled criterion, so that the large spherical voids nucleate relatively early, as soon as the stresses grow large. At the small particles, represented by f_N^o, nucleation occurs according to a strain controlled criterion, so that large strains are required before the small-scale voids appear.

Results of two computations, for $b = 0$ and $b = 1$, respectively, in (1) are illustrated in Fig. 8 by the development of the void volume fraction at

five different points of the region analysed and the maximum principal logarithmic strain at two points vs. the macroscopic logarithmic strain ϵ_{II} in the x^1-direction. On the macroscopic level the material is subjected to uniaxial plane strain tension, with $\epsilon_{III} = 0$ and $\Sigma_{II} = 0$, and the mesh used consists of $7\times7\times3$ box super elements, where the smaller resolution is in the x^3-direction.

In the initial stage the two strain values shown in Fig. 8b remain nearly identical, but then they start to differ, and at some stage localization of plastic flow occurs. The onset of elastic unloading is indicated by an arrow on the curves, and ψ_u is the angle of inclination of the diagonal at unloading. When elastic unloading reaches point A, soon after the initial elastic unloading, ϵ_A becomes constant, while the peak strain ϵ_B inside the shear band starts to grow much more rapidly. It is seen that somewhat earlier localization is predicted by the kinematic hardening model than by the isotropic hardening model. The value f_0 of the void volume fraction is taken inside the "island" of additional stress controlled nucleation, and here the porosity increases rapidly, leading to a large soft-spot that grows into one of the larger voids. The circle at the end of the curve indicates the point where the first final failure occurs in one of the 24 tetrahedral elements of the box element. The values f_X and f_Y represent points outside the shear band, where the void volume fraction is constant after that elastic unloading occurs and remains relatively low. Both f_B and f_Z are inside the shear band, and these values grow rapidly towards final failure after the onset of localization. Due to the symmetries assumed here, two shear bands cross through the region represented by f_Z, and therefore f_Z grows more rapidly than f_B. The 3D aspects of the computation are most clearly illustrated by the difference between f_0 and f_Z in Fig. 8a. If plane strain was assumed throughout the material, f_Z would be identical to f_0 by definition.

Computations using this 3D material model have also been carried out for a higher level of stress triaxiality $\Sigma_{II}/\Sigma_I = 0.25$, and for a macroscopic strain state that deviates from plane strain, as specified by $\epsilon_{III}/\epsilon_{II} = 0.5$. In all these computations the radius r_0 of the larger inclusions (25) is chosen corresponding to a volume fraction 0.01 and the volume fraction of small scale particles is taken to be 0.04. The width of the region analysed is taken to be $C_0 = \sqrt{A_0 B_0}$, and the value of the aspect ratio A_0/B_0 is chosen such that the angle of inclination of the diagonal is close to the critical angle for shear bands when localization wants to occur. This means that the periodic pattern analysed is chosen representative of the most critical relative location of larger voids, for which failure by shear localization between two larger voids is first critical.

The $7\times7\times3$ mesh used for these 3D numerical analyses is rather crude. Some insight in the effect of a mesh refinement is gained from a comparison with plane strain results, which indicate that a finer mesh in the coordinate plane normal to the shear band (the x^1-x^2-plane) will give earlier locali-

zation, mainly because the strain concentrations around the larger voids are better resolved. At the same time such a finer mesh would allow for a more narrow shear band, which would lead to a smaller overall strain at final failure. Furthermore, 3D computation with a 7x7x5 mesh show that the results are not very sensitive to a mesh refinement in the sideways direction along the shear band (the x^3-direction).

BRITTLE DUCTILE TRANSITION

The transition from a low absorbed fracture energy to a high absorbed energy in structural alloys is characterized by a competition between a brittle failure mode and a ductile failure mode. Ductile fracture with the associated high energy absorption occurs by void coalescence, while in body-centered-cubic (b.c.c.) metals failure in the low temperature range occurs by cleavage. Tvergaard and Needleman (1986) have used an extended version of the porous ductile material model to study this fracture mode transition.

Strain-rate sensitive material model

Failure by cleavage is included in the material model in a relatively simple manner, by assuming that failure occurs if the maximum principal tensile stress exceeds a certain critical value σ_C

$$\text{Max}(\sigma_1 \, , \, \sigma_2 \, , \, \sigma_3) \geq \sigma_C \tag{26}$$

Such a constant critical stress has been found to be a realistic criterion for slip induced cleavage failure in b.c.c. metals at low temperatures (Cottrell, 1958; Petch, 1958; Hahn, 1984). The criterion may be less accurate at higher temperatures near the transition to fibrous fracture, where final link-up of the cleavage micro-cracks requires further plastic deformations; but it has been assumed (Tvergaard and Needleman, 1986,1988) that a constant value of σ_C in (26) is a sufficiently good criterion in the temperature range considered.

In addition to cleavage fracture it is also important to incorporate material strain-rate sensitivity in the material model, since this accounts for the difference between the transition temperature at slow loading and that at impact loading. Rate sensitivity is incorporated in the ductile porous material model (Pan, Saje and Needleman, 1983) by representing the matrix material as elastic-viscoplastic. The microscopic effective plastic strain-rate $\dot{\epsilon}^P_M$ is represented by the power law relation

$$\dot{\epsilon}^P_M = \dot{\epsilon}_o \left[\frac{\sigma_M}{g(\epsilon^P_M)} \right]^{1/m} \tag{27}$$

where m is the strain-rate hardening exponent, $\dot{\epsilon}_o$ is a reference strain-rate, and $(\dot{})$ denotes the time derivative in this time-dependent material model. The function $g(\epsilon^P_M)$ represents the effective tensile flow

stress in the matrix material in a tensile test carried out at a strain-rate such that $\dot{\epsilon}^P_M = \dot{\epsilon}_o$. For a power hardening material with strain hardening exponent n and reference stress σ_o the function $g(\epsilon^P_M)$ is given by

$$\epsilon^P_M = \frac{\sigma_o}{E} \left[\left\{ \frac{g(\epsilon^P_M)}{\sigma_o} \right\}^n - \frac{g(\epsilon^P_M)}{\sigma_o} \right] \quad , \quad g(0) = \sigma_o \tag{28}$$

In the elastic-viscoplastic material model the function $\Phi(\sigma^{ij} \, , \, \sigma_M \, , \, f) = 0$ given by (2) for $b = 1$ is used as a plastic potential, so that the inelastic part of the macroscopic strain-rate is given by

$$\dot{\eta}^P_{ij} = \Lambda \frac{\partial \Phi}{\partial \sigma^{ij}} \tag{29}$$

Furthermore, equality of the macroscopic plastic work rate with the microscopic dissipation ((5) for $b = 1$) is assumed, and this requirement together with (29) gives

$$\Lambda = (1-f)\sigma_M \, \dot{\epsilon}^P_M \left[\sigma^{ij} \frac{\partial \Phi}{\partial \sigma^{ij}} \right]^{-1} \tag{30}$$

The rate of increase of the void volume fraction is still assumed to be given by (8) and (9), with the expression (10) for the rate of nucleation replaced by

$$(\dot{f})_{\text{nucleation}} = \mathcal{B} \left[\dot{\sigma}_M + (\sigma^k_k)^{\cdot}/3 \right] + \mathcal{D} \, \dot{\epsilon}^P_M \tag{31}$$

This different expression for the nucleation of new voids is necessary to represent plastic strain controlled nucleation, since in the viscoplastic material model there is no one to one relationship between $\dot{\epsilon}^P_M$ and $\dot{\sigma}_M$. Finally, to determine the values of $\dot{f}$ and $\dot{\sigma}_M$ the consistency condition $\dot{\Phi} = 0$ is needed in each increment.

The total macroscopic strain-rate is taken to be the sum of the elastic and inelastic parts, $\dot{\eta}_{ij} = \dot{\eta}^E_{ij} + \dot{\eta}^P_{ij}$, as in the time-independent model, and it is noted that in the limit $m \to 0$ the elastic-viscoplastic material model reduces exactly to the time-independent porous material model for $b = 1$. A kinematic hardening version ($b < 1$) of this viscoplastic material model has been discussed by Becker and Needleman (1986).

The Charpy V-notch test

A measure of the fracture mode transition in structural alloys is traditionally obtained in terms of the energy absorbed in the Charpy V-notch test. An alternative measure is the temperature dependence of the critical value of the stress intensity factor K_{Ic} for a sharp crack, or K_{Id} in the case of dynamic loading. Relations between these measures have been

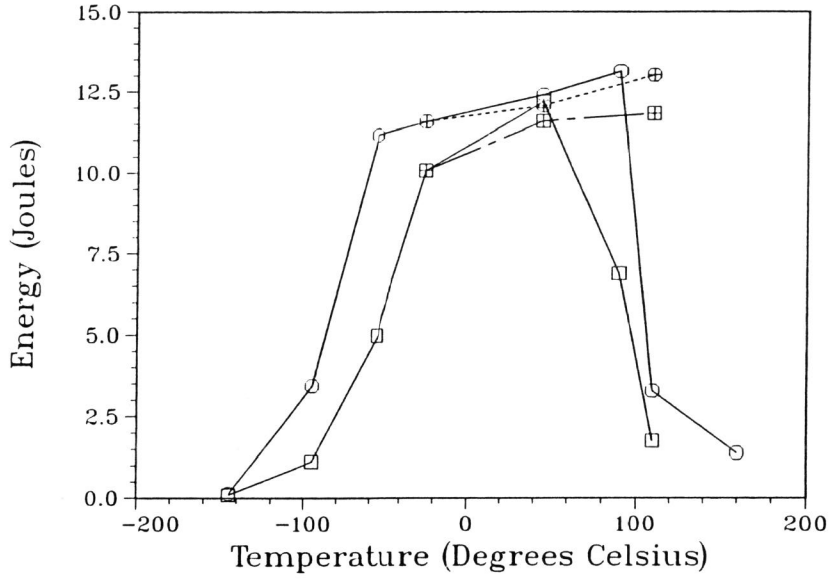

Fig. 9. Computed curves of absorbed energy vs. temperature for a high nitrogen steel. O low imposed velocity, $5 \cdot 10^{-4}$ m/sec . □ impact, 5 m/sec (Tvergaard and Needleman, 1988).

discussed by a number of authors (e.g. see Rolfe and Barsom, 1977).

Numerical studies of the transition in the Charpy V-notch test have been carried out by Tvergaard and Needleman (1986,1988). The first investigation focused on the effect of different strain-rates at a constant temperature, thus comparing the behaviour at slow bending with that at impact loading. It was found that the viscoplastic porous material model, extended by the simple representation (26) of cleavage failure, is able to reproduce the experimentally observed behaviour. An increased loading rate can indeed result in a transition from fibrous fracture initiation to fracture initiation by cleavage, associated with a reduced energy absorption. The results also indicate agreement with the experimental observation that on the upper shelf, where fibrous fracture is dominant, the absorbed energy is larger at impact loading than at slow loading, due to the rate dependent difference in the apparent yield stress.

In a more recent investigation (Tvergaard and Needleman, 1988) the temperature dependence of the absorbed energy predicted by the material model has been computed for a particular material, the high-nitrogen mild steel studied by Ritchie, Knott and Rice (1973). The temperature dependence of the initial yield stress is given by Ritchie *et al.* (1973) and the additional specification of the ultimate tensile stress makes it possible to estimate the temperature dependence of the strain hardening exponent; but still the assumption of simple power hardening at all temperatures may be a crude approximation. Furthermore, the value of the rate hardening exponent m

was not specified in the experimental investigation, but was taken in the computations to be constant at a value m = 0.01 , representative for mild steels.

Fig. 9 shows computed absorbed energies for two different imposed velocities, $5 \cdot 10^{-4}$ m/sec and 5 m/sec , respectively, at the mid point of the specimen where the pendulum hits. It is seen that the brittle ductile transition is predicted at -85° and -50° for slow loading and impact loading, respectively, while a rather untypical behaviour is found at temperatures above 45° , due to the development of "blue brittleness" for this material. In fact, the strongly increasing strain hardening for increasing temperature plays an important role, so that even at the upper shelf found in Fig. 9 the two failure modes remain in close competition. Therefore, the predictions may be rather sensitive to changes of the estimated material parameters.

In addition to the quasi-static analyses, a few computations have been repeated as dynamic analyses (Tvergaard and Needleman, 1988), taking full account of inertia. Although these analyses show strong oscillations of the contact force between pendulum and specimen, the absorbed energies found are in good agreement with the predictions of the quasi-static analyses.

CONCLUDING REMARKS

The current understanding of porous ductile material behaviour relies on micro-mechanical modelling as well as experiments. Here, the focus has been on theoretical modelling, regarding the apparent dilatant plasticity on the macroscopic level, as well as the representation of more complex fracture mechanisms. This includes localization of plastic flow in shear bands, the interaction of two size scales of voids, or void growth involving contact between the void surface and a second phase particle inside the void.

For experimental investigations powder compacts sintered to various known levels of porosity are very useful. In these materials the distribution of porosity is reasonably uniform with known void volume fraction, and since nucleation of new voids is not an issue, the effect of void growth is tested separately in such experiments. In addition to tests for uniaxial tension or compression (e.g. see discussion by Tvergaard, 1987a), a detailed comparison of theoretical and experimental results for notched tensile specimens has been carried out recently by Becker *et al.* (1988). This comparison is particularly interesting, because it covers both void growth and final failure mechanism in a strongly non-uniform strain field.

The correlation of nucleation with strains or stresses for a given alloy must still be obtained from experiments. However, micro-mechanical studies can give important information about particular effects, such as decohesion mechanisms, the influence of nucleation on macroscopic behaviour, and the importance of particle matrix contact after nucleation.

REFERENCES

Becker, R. and Needleman, A. (1986). Effect of yield surface curvature on necking and failure in porous plastic solids. J. Appl. Mech. 108, 491-499.

Becker, R., Needleman, A., Richmond, O. and Tvergaard, V. (1988). Void growth and failure in notched bars. J. Mech. Phys. Solids 36, 317-351.

Bishop, J.F.W. and Hill, R. (1951). A theory of the plastic distortion of a polycrystalline aggregate under combined stresses. Phil. Mag. 42, 414-427.

Chu, C.C. and Needleman, A. (1980). Void nucleation effects in biaxially stretched sheets. J. Eng. Materials Technol. 102, 249-256.

Cottrell, A.H. (1958). Theory of brittle fracture in steel and similar metals. Transactions AIME 212, 192-203.

Dafalias, Y.F. (1983). Corotational rates for kinematic hardening at large plastic deformations. J. Appl. Mech. 50, 561-565.

Fleck, N.A. and Hutchinson, J.W. (1986). Void growth in shear. Proc. Roy. Soc. Lond. A 407, 435-458.

Fleck, N.A., Hutchinson, J.W. and Tvergaard, V. (1988). Softening by void nucleation and growth in tension and shear. Division of Applied Sciences, Harvard University.

Guennouni, T. and Francois, D. (1987). Constitutive equations for rigid plastic or viscoplastic materials containing voids. Fatigue Fract. Engng. Mater. Struct. 10, 399-418.

Gurson, A.L. (1977). Continuum theory of ductile rupture by void nucleation and growth - I. Yield criteria and flow rules for porous ductile media. J. Engng. Materials Technol. 99, 2-15.

Hahn, G.T. (1984). The influence of microstructure on brittle fracture toughness. Metallurgical Transactions 15A, 947-959.

Hahn, G.T. and Rosenfield, A.R. (1975). Metallurgical factors affecting fracture toughness of aluminum alloys. Met. Trans. 6A, 653-668.

Hancock, J.W. and MacKenzie, A.C. (1976). On the mechanisms of ductile failure in high strength steels subjected to multiaxial stress-states. J. Mech. Phys. Solids 24, 147-169.

Hutchinson, J.W. and Tvergaard, V. (1987). Softening due to void nucleation in metals. Harvard University, Division of Appl. Sci., Mech-99.

Lee, E.H., Mallett, R.L. and Wertheimer, T.B. (1983). Stress analysis for kinematic hardening in finite-deformation plasticity. J. Appl. Mech. 50, 554-560.

Magnusen, P.E., Koss, D.A. and Dubensky, E.M. (1987). Ductile fracture and random vs. regular hole/void arrays. Office of Naval Research, N00014-86-K-0381, Techn. Rep. No. 5.

Mear, M.E. and Hutchinson, J.W. (1985). Influence of yield surface curvature on flow localization in dilatant plasticity. Mechanics of Materials 4, 395-407.

Needleman, A. (1972). Void growth in an elastic-plastic medium. J. Appl. Mech. 41, 964-970.

Needleman, A. and Rice, J.R. (1978). Limits to ductility set by plastic flow localization. in Mechanics of Sheet Metal Forming (eds. D.P. Koistinen *et al.*), 237-267, Plenum Publishing Corporation.

Pan, J., Saje, M. and Needleman, A. (1983). Localization of deformation in rate sensitive porous plastic solids. Int. J. Fracture 21, 261-278.

Petch, N.J. (1958). The ductile-brittle transition in the fracture of α-iron: I. Philosophical Magazine 3, 1089-1097.

Ritchie, R.O., Knott, J.F. and Rice, J.R. (1973). On the relationship between critical tensile stress and fracture toughness in mild steel. J. Mech. Phys. Solids 21, 395-410.

Rolfe, S.T. and Barsom, J.M. (1977). Fracture and Fatigue Control in Structures - Applications of Fracture Mechanics. Prentice Hall, Englewood Cliffs NJ.

Tvergaard, V. (1981). Influence of voids on shear band instabilities under plane strain conditions. Int. J. Fracture 17, 389-407.

Tvergaard, V. (1982a). On localization in ductile materials containing spherical voids. Int. J. Fracture 18, 237-252.

Tvergaard, V. (1982b). Ductile fracture by cavity nucleation between larger voids. J. Mech. Phys. Solids 30, 265-286.

Tvergaard, V. (1982c). Influence of void nucleation on ductile shear fracture at a free surface. J. Mech. Phys. Solids 30, 399-425.

Tvergaard, V. (1987a). Effect of yield surface curvature and void nucleation on plastic flow localization. J. Mech. Phys. Solids 35, 43-60.

Tvergaard, V. (1987b). 3D-analysis of localization failure in a ductile material containing two size-scales of spherical particles. Technical University of Denmark, DCAMM Report No. 365.

Tvergaard, V. and Needleman, A. (1984). Analysis of the cup-cone fracture in a round tensile bar. Acta Metallurgica 32, 157-169.

Tvergaard, V. and Needleman, A. (1986). Effect of material rate sensitivity on failure modes in the Charpy V-notch test. J. Mech. Phys. Solids 34, 213-241.

Tvergaard, V. and Needleman, A. (1988). Temperature and rate dependence of Charpy V-notch energies for a high nitrogen steel. Int. J. Fracture 37, 197-215.

Tvergaard, V., Needleman, A. and Lo, K.K. (1981). Flow localization in the plane strain tensile test. J. Mech. Phys. Solids 29, 115-142.

Ziegler, H. (1959). A modification of Prager's hardening rule. Quart. Appl. Math. 17, 55-65.